Experimental Evidence of Acoustic Shock Wave-Induced Dynamic Recrystallization: A Case Study on Ammonium Sulfate

Sivakumar Aswathappa, Lidong Dai,* S. Sahaya Jude Dhas, S. A. Martin Britto Dhas, Eniya Palaniyasan, Raju Suresh Kumar, and Abdulrahman I. Almansour

Cite This: *Cryst. Growth Des.* 2024, 24, 491–498

Read Online

ACCESS | Metrics & More | Article Recommendations | Supporting Information

ABSTRACT: Here, we present the findings of acoustic shock wave processing inflicted on ammonium sulfate powder samples and demonstrate the unique phenomenon of dynamic recrystallization occurring because of the superheating of the surface within the span of milliseconds. The results of X-ray diffraction (XRD) and field emission scanning electron microscopy (FE-SEM) clearly reveal the linear enhancement of the intensity ratio of the planes (200)/(120) and (200)/(111) under shocked conditions, and the observed results of dynamic recrystallization are highly relevant to the attachment energy theory of crystallization.
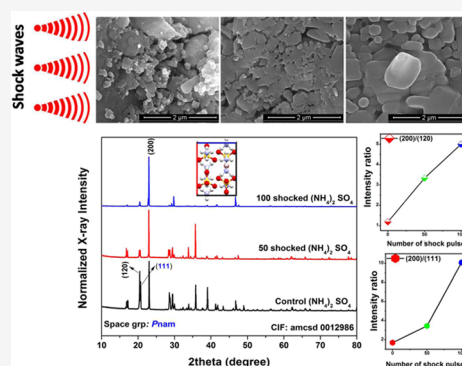
INTRODUCTION

Research on functional materials, especially on fundamental concepts, is always focused on enhancing our understanding of material properties toward practical applications, and hence, reliable experiments are highly required for the development of science and technology. In view of this, studies on nucleation, crystal growth, and phase transformations are fundamental prerequisites in understanding various concepts of solid-state Physics since these relate to the genesis and evolution of novel microstructures[1,2], which have different characteristics in steady-state and unsteady-state thermodynamic conditions.[3,4] The mechanisms of nucleation, crystal growth, and phase transitions are well-understood under steady-state thermodynamic conditions, whereas a clear understanding of unsteady-state thermodynamic conditions is yet to be formulated, which include laser shock waves,[5,6] flyer plate shock compression,[7,8] and acoustical shock waves.[9,10] Conventional heating experiments by diamond-anvil cells (DACs) essentially fall under steady-state processes.[3] Techniques such as laser shock waves[5,6] and flyer plate shock compression[7,8] are capable of producing high pressure and temperature simultaneously on the test sample's surface within 10^{-9} S, whereby a majority of materials undergo premelting and dynamic recrystallization during the formation of rarefaction waves.[5–8] Millisecond shock wave (acoustical shock wave) processing is one of the most promising high-pressure techniques. Under shocked conditions, most of the materials undergo structural deformations, whereas a few materials experience solid-state phase transitions because of the dynamic recrystallization within milliseconds, which is much lower than the laser shock

waves and the flyer plate dynamic shock compression processes[11–13] and much higher than that of the DAC technique.[3,4] According to the literature, dynamic heating (superheating) caused by shock loading is a dominant feature compared to static heating.[11–13] Although the possibility of acoustical shock wave-induced solid-state phase transitions occurring on materials such as from crystal to crystal,[11] crystal to amorphous,[12] and amorphous to crystal[12] has been witnessed, enhancements of the optical transmittance,[14] thermal diffusivity,[15] and dielectric constant[16] have also been observed, which are because of the dynamic recrystallization. In general, several theories and reports have contributed to the fundamental stability limits of superheated solids, revealing that most of the materials cannot maintain the crystalline order under shocked conditions, which greatly depends not only on the critical time required for phase transitions as well as the structural relaxation time but also on the temperature and pressure.[17–19] Shock melting experiments are highly useful for studying the high-pressure melting of geophysical and physically important materials, and morphological studies on shock wave-recovered samples can give a better understanding of the unsteady-state characteristic features of materials, which could help in realizing several unknown solid-state phenomena.
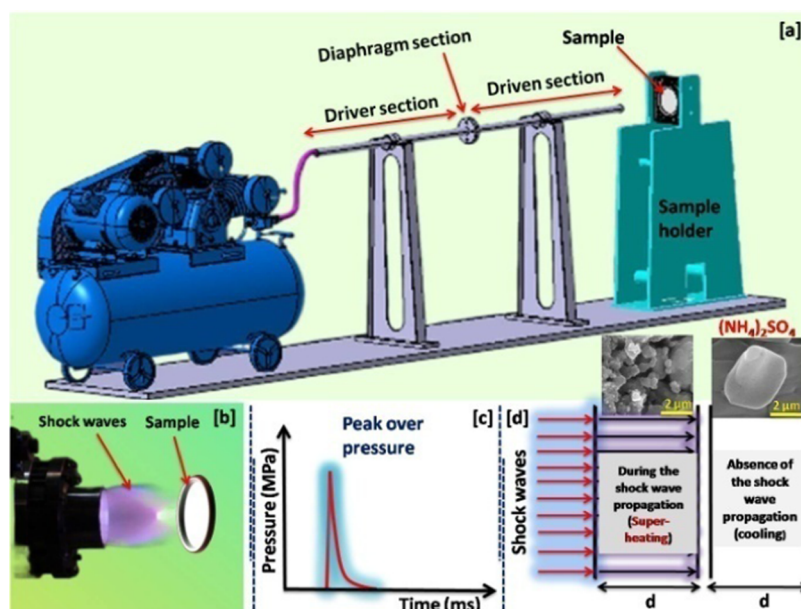
Figure 1. Schematic diagram of the shock wave-loading technique.
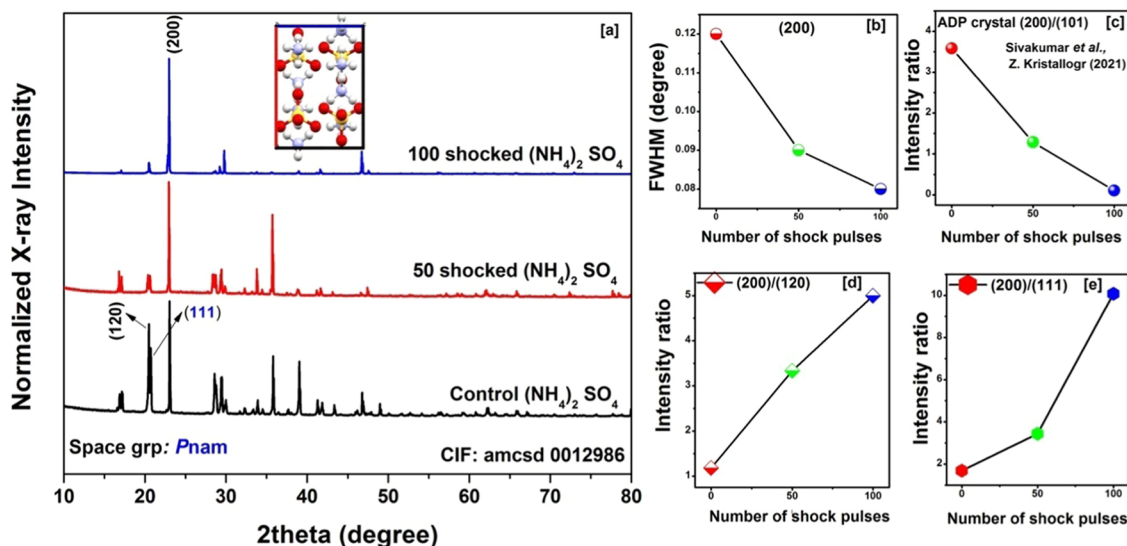
Figure 2. (a) XRD patterns of the control and shocked AS samples, (b) FWHM of the (200) plane, and (c) normalized intensity ratio of (200)/(120) and (d) (200)/(111) with respect to the number of shock pulses.

In the present study, ammonium sulfate $(NH_4)_2SO_4$ (henceforth represented as "AS") is chosen to demonstrate shock wave-induced dynamic recrystallization since it is one of the classical materials and well-explored under steady-state thermodynamic conditions.[20−22] We attempt here to reconcile the issues related to shock wave-assisted melting and recrystallization occurring in milliseconds and at lower heating rates, wherein a lot of discrepancies are found between the results of steady-state melting. The shocked test samples have a highly ordered crystalline prismatic face of the (200) plane with a well-defined surface morphology against the control sample.

■ EXPERIMENTAL SECTION

The test crystal's growth details and the features of the shock tube and its mechanism[23] as well as the shock wave-loading procedures are presented in the Supporting Information. Briefly, in the present experiment, three AS powder samples of equal amounts (the as-grown single crystal was crushed to a powder form) have been chosen, and one sample has been kept as the control and the rest of the two samples have been utilized for the shock wave recovery experiments. In the present prospect, the shock waves of Mach number 2.2 have been utilized, which possess a transient temperature of 846 K and transient pressure of 2.0 MPa. 50 and 100 shock pulses have been applied to the two samples, and thereafter, X-ray diffraction (XRD), Raman, ultraviolet diffuse reflectance spectroscope (UV-DRS), and field emission scanning electron microscopy (FE-SEM) studies have been performed for the control and shocked samples, after which the results are compared. The schematic diagram of the shock wave-loading technique is presented in Figure 1.

The analysis of powder X-ray diffraction (PXRD) [Rigaku-Smart Lab X-ray diffractometer, Japan, Cu Kα_1 as the X-ray source (λ = 1.5407 Å), with the step precision of $\pm$0.001°] was performed. A Renishaw model Raman spectrometer with laser line 532 nm and power 50 mW and Raman measurement was carried out using the pelletized form of samples. The laser spot size was 50 μm^2, and the
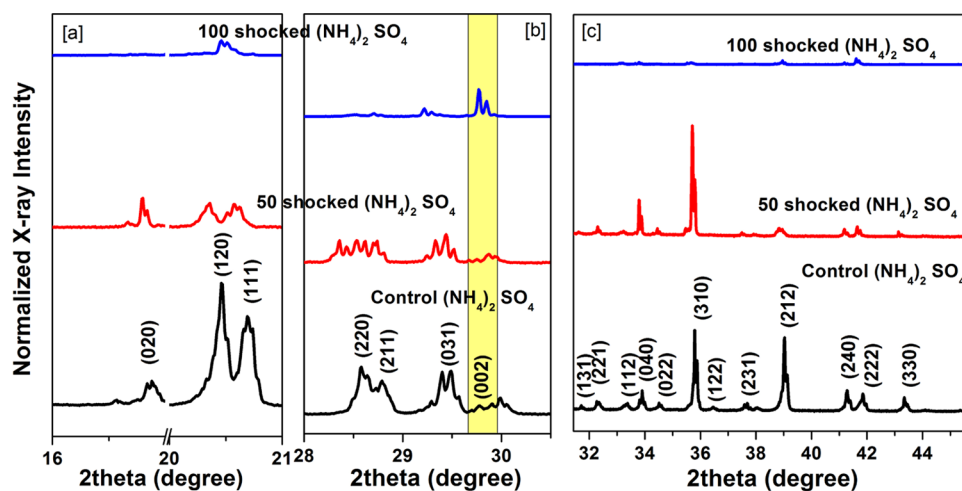
Figure 3. (a) XRD patterns of the control and shocked AS samples 16−21°, (b) 28−30.5°, and (c) 31.5−43°.

optical microscope's objective lens was used; an X50 long working distance objective lens (WD = 10.6 mm) was utilized, and the value of the numerical aperture was 0.5, while the Raman data were collected by Renishaw Wire 5.1 instrument control and data acquisition software. An ultraviolet diffuse reflectance spectroscope (UV-DRS ShimadzuUV-3600 plus) was utilized to understand linear optical properties. A field emission scanning electron microscope (Carl Zeiss FE-SEM, Sigma 300, Schottky FEG) operating at an acceleration voltage of 10 kV was used to analyze the morphology of the title material.

RESULTS AND DISCUSSION

XRD Results. Figure 2a shows the control and shocked samples' XRD patterns, wherein the control sample's XRD patterns are identified to be well-matched with previous reports[20] and the CIF file: amcsd0012986. Based on the obtained XRD patterns of the control sample, it is crystallized in the orthorhombic structure with the space group *Pnam* and the lattice dimensions are a = 7.782, b = 10.636, and c = 5.993 Å. For better image clarity, only the dominant diffraction lines such as (120), (111), and (200) planes are indexed, while the completely indexed XRD patterns are presented in Figure 3. At the initial screening of the XRD patterns, the number of crystalline planes, the full width at half-maximum (fwhm), and the normalized intensity ratio of the XRD peaks are significantly changed with respect to the number of shock pulses. On the one hand, the fwhm value of the dominant diffraction peak (200) increased linearly when increasing the number of shock pulses from 0 to 100, and the required XRD profile is presented in Figure 2b. Moreover, the XRD peaks' intensity ratios for (200)/(120) and (200)/(111) increased linearly with respect to the number of shock pulses, and the required plots are portrayed in Figure 2c,d. On the other hand, based on the XRD results in Figure 2a−d, it is clear that the intensity of both the bi-indexed plane (120) and the tri-indexed plane (111) significantly reduced, whereas a rapid enhancement was found for the plane (200) because of the dynamic recrystallization.

On those counts, the observed results could be elaborated based on the standard attachment energy theory of crystallization, whereby the attachment energy is always directly proportional to the growth rate of the plane.[24−26] Based on the available values of the attachment energy of the AS crystal,[24] the (200) plane has a higher growth rate than the

other planes as the corresponding attachment energy is −87.38 kcal/mol, whereas the attachment energy for the (001) plane is −48.25 kcal/mol. During the shock wave-loaded conditions, sudden impulsion of high-temperature shock pulse on the AS crystal surface is experienced, whereby superheating occurs within milliseconds and immediately rapid cooling (after a few milliseconds) takes place; thus, the surface comes to a region of low temperature, and this kind of superheating and cooling process initiates a significant dynamic recrystallization process from the molten state of the test sample, which is a prestate of the conventional melting process.

Note that, due to the short heating time as well as heat dissipation, the test sample does not undergo the conventional melting process even though the shock pulse supplies enough temperature to melt the test sample, whereas in such shocked conditions, the test sample may undergo the molten state during the heating process and recrystallize during the cooling process, and this cyclic process repeatedly happens at every shocked condition. While the test sample comes from the molten state to the solid state, the attachment energy of the facets plays a vital role such that usually the higher attachment energy planes can easily crystallize compared to the other planes, and hence, in the present case, intensities of planes (120) and (111) are tremendously reduced, but a rapid enhancement was found for the (200) plane. As observed, the enhancement of the intensity ratio, as shown in Figure 2c,d, is linearly increased while increasing the number of shock pulses, and the obtained results clearly show that the degree of recrystallization increases linearly when increasing the number of shock pulses. The observed results are found to be in good agreement with the attachment energy theory of crystallization[24−26] and the previously obtained shock wave-induced results of structural properties.[27,28] To draw a parallel line, shocked samples of ammonium dihydrogen phosphate (ADP) and potassium dihydrogen phosphate (KDP) polycrystalline are considered for a better comparative analysis of the observed results. Note that the ADP and KDP crystals have two dominant planes that are (200) and (101), respectively, with the respective growth rates of 2.21 and 2.25. In addition, the attachment energies of the (200) and (101) planes for the KDP crystal are 36 and 101 kcal/mol, respectively,[29] and hence, under shocked conditions, the (101) peak intensity increases with respect to the number of shock pulses;[28] similar results have been observed for the ADP crystal under shocked
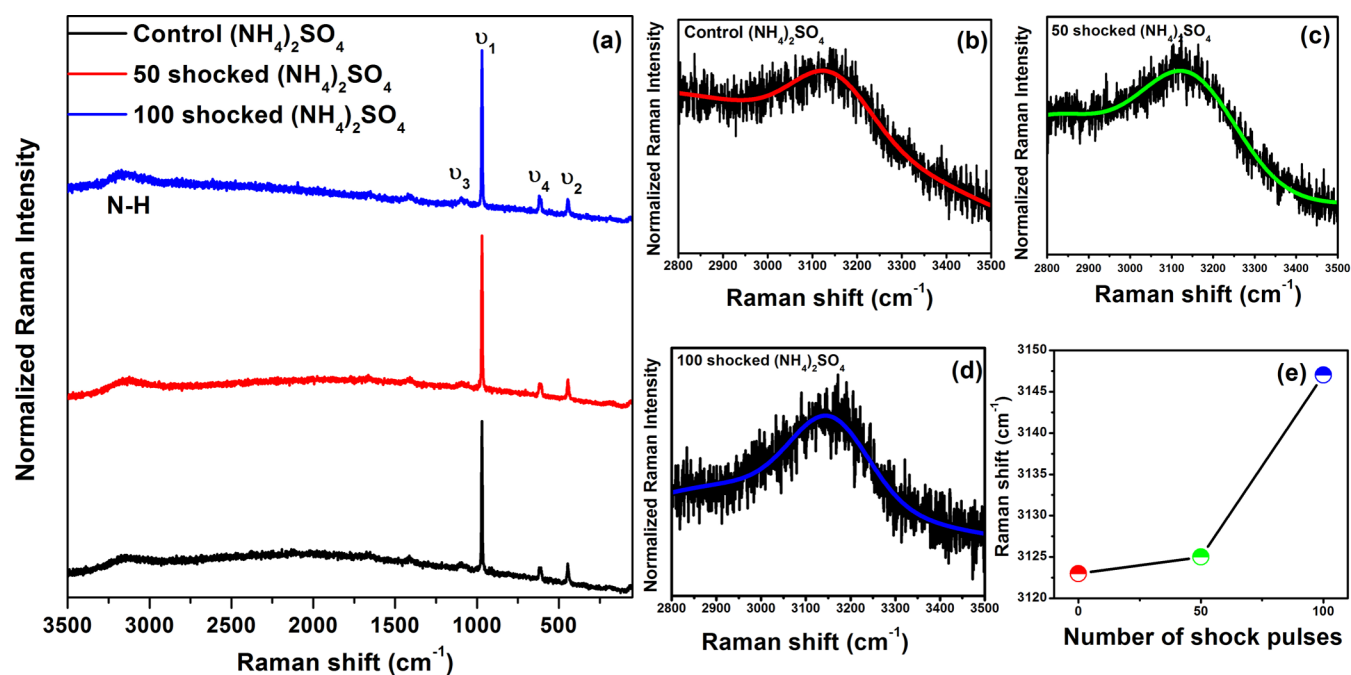
Figure 4. (a) Raman spectra of the control and shocked AS samples. (b) N−H Raman band for the control sample. (c) N−H Raman band for the 50-shocked sample. (d) N−H Raman band for the 100-shocked sample. (e) Raman shift of the N−H band with respect to the number of shock pulses.
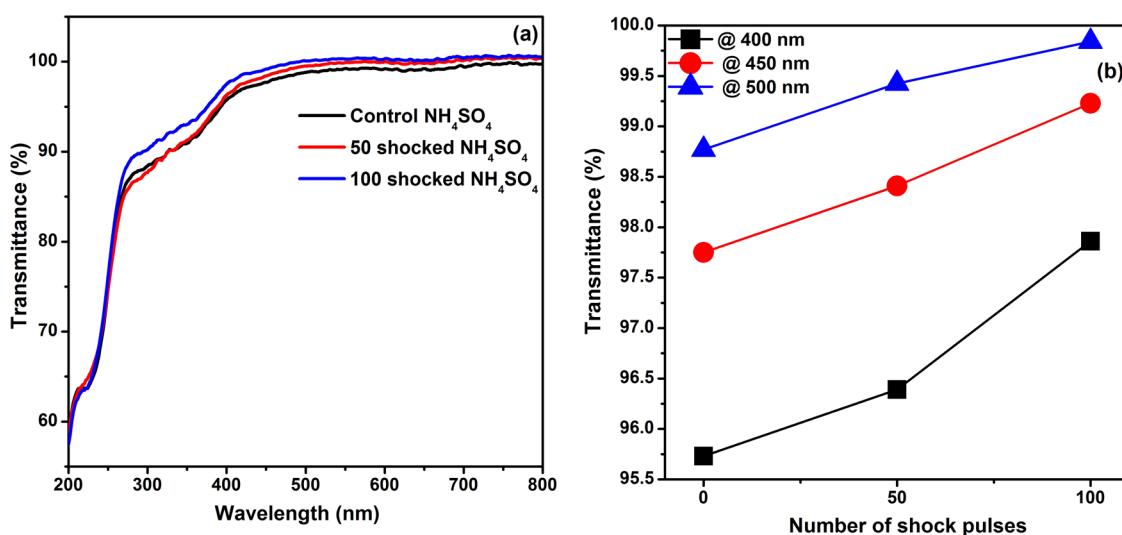
Figure 5. (a) Optical transmittance of the control and shocked AS samples. (b) Optical transmittance percentage at 400, 450, and 500 nm regions with respect to the number of shock pulses.

conditions, and the values of the intensity ratio for the (200)/(101) plane are presented in Figure 2d with respect to the number of shock pulses.[27]

Raman Spectroscopic Results. The complete Raman spectral results of the control and shocked AS samples are presented in Figure 4a, wherein the control sample has the characteristic SO_4 and NH_4 Raman bands, which are found to be in good agreement with previous reports.[30,31] However, compared to the SO_4 Raman bands, NH_4 bands have a lower Raman intensity because of the lower scattering geometry. No significant modification was found in the SO_4 cationic Raman band positions and shapes of v_1, v_2, v_3, and v_4, whereas a considerably higher energy Raman shift was noted in the NH_4 Raman modes. To extract possible supporting shreds of

evidence for the XRD from the Raman results, the zoomed-in versions of the N−H Raman band regions for the control and shocked samples are displayed in Figure 4b−d, wherein the N−H Raman band is located at 3123 cm^{-1} for the control sample, which got shifted toward higher wavenumbers to be located at 3125 and 3147 cm^{-1} for the respective 50- and 100-shocked conditions, and the required plot is presented in Figure 4e. In addition, the normalized N−H Raman band values are 0.204, 0.154, and 0.276 for the 0, 50, and 100-shocked AS samples, respectively, and analysis of the higher Raman band intensity at the 100-shocked condition clearly shows that the formation of a higher degree of crystalline AS sample at the 100-shocked condition is based on the shock wave-induced dynamic recrystallization and UV-DRS results
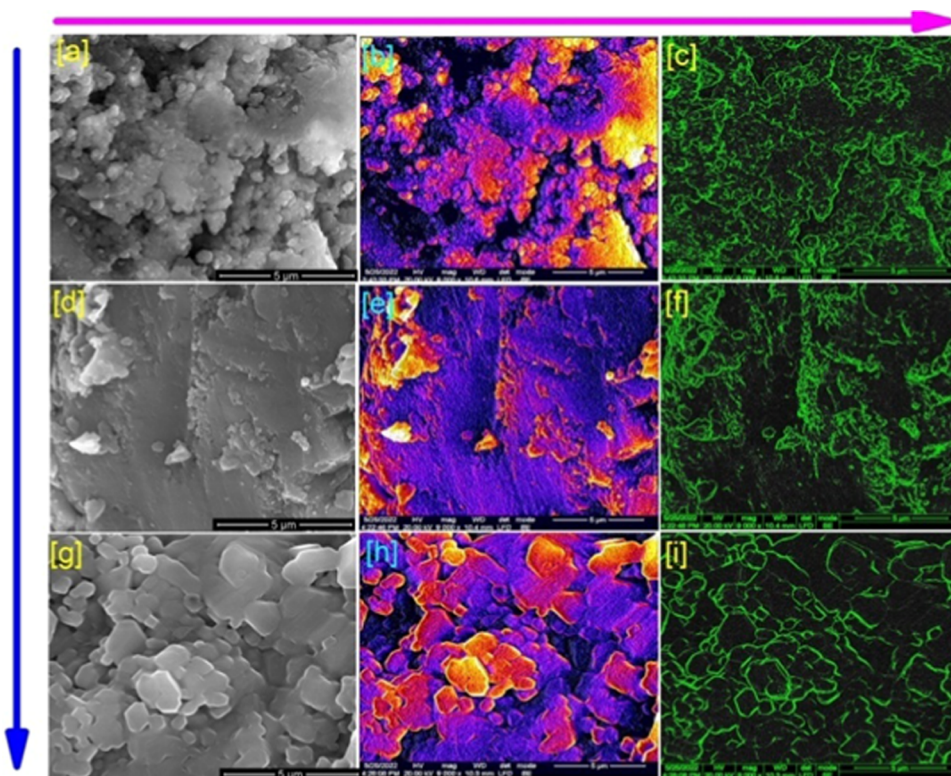
Figure 6. FE-SEM images (5 μm-scale resolution) of the control and shocked AS samples: (a–c) control, (d–f) 50-shocked samples, and (g–i) 100-shocked samples.
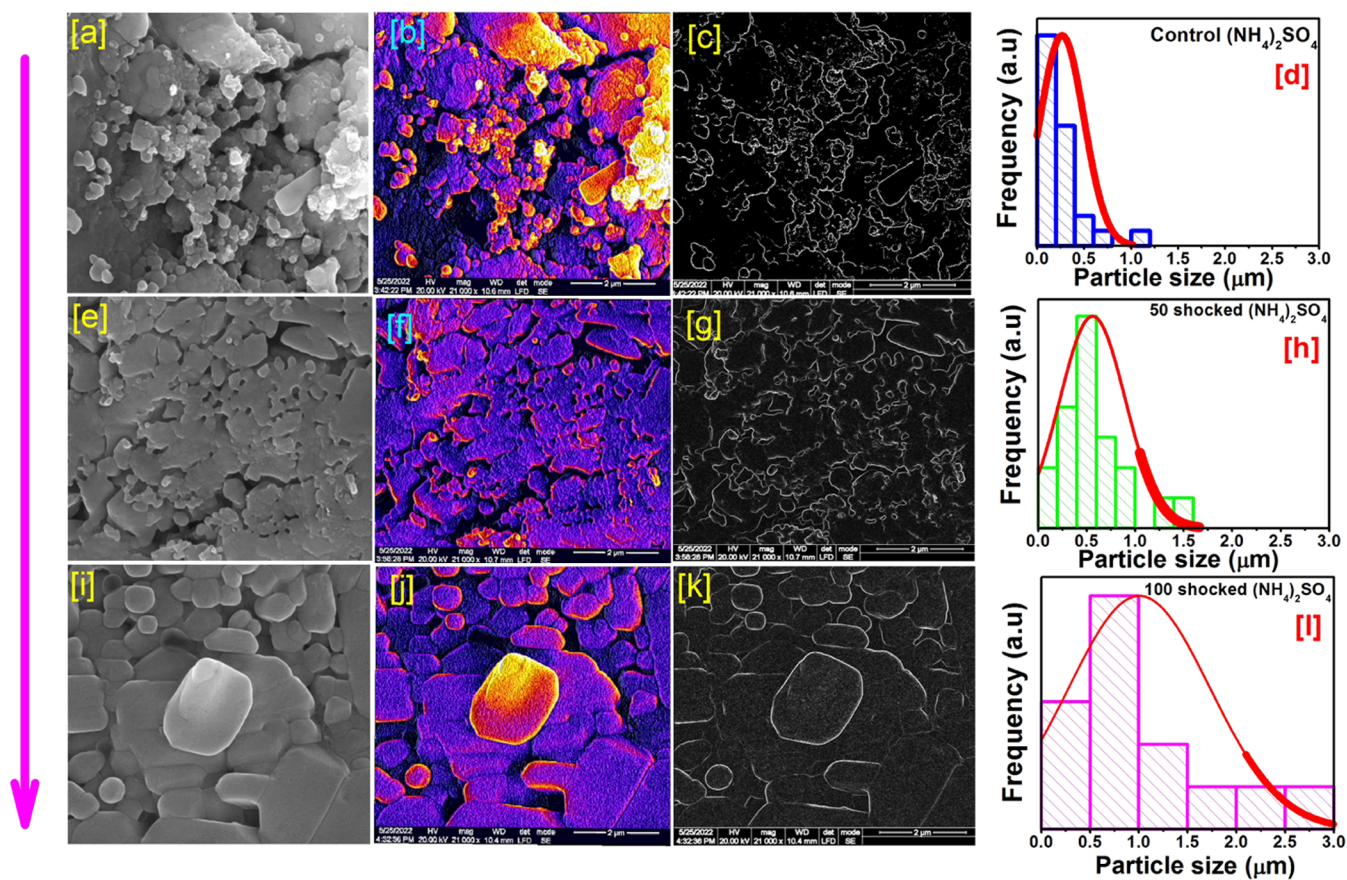
Figure 7. FE-SEM images (2 μm-scale magnification) of the control and shocked AS samples: (a–c) control, (d–f) 50-shocked samples, and (g–i) 100-shocked samples.
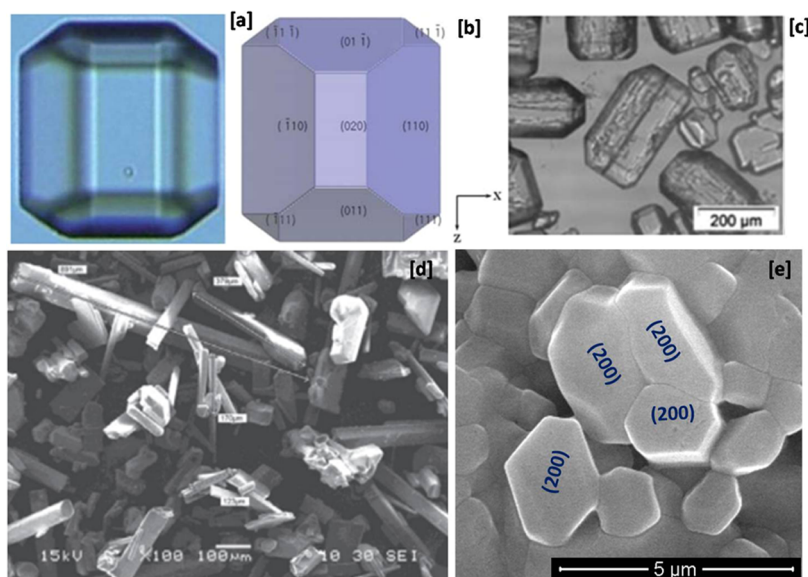
Figure 8. SEM images of the AS samples: (a, b) crystal morphology with nomenclature of specific faces,[22] (c) conventional crystal growth of AS sample (adopted reprint permission),[22] (d) ultrasonic wave-assisted AS sample,[33] and (e) present work.

(Figure 5a,b), which are in agreement with the XRD and Raman results, and the detailed discussion has been provided in the Supporting Information.

UV-DRS Results. The control and shocked AS samples' optical transmittance profiles are presented in Figure 5a, which can provide supporting evidence for the reduction of grain boundary density and enhancement of the net degree of crystalline nature of the test sample. The control sample's optical transmittance spectrum is found to be well-matched with the previously reported AS samples.[32]

As seen by the naked eye, a considerable enhancement of the optical transmittance and blue shift of the upper cutoff absorption edge with respect to the number of shock pulses could be witnessed. For a clear understanding of the enhancement of the optical transmittance of AS samples under shocked conditions, the optical transmittance percentage is measured at three different wavelength regions such as 400, 450, and 500 nm; the measured values of the optical transmittance are displayed in Figure 5b with respect to the number of shock pulses. Figure 5b clearly demonstrates that the linear enhancement of the optical transmittance with respect to the number of shock pulses is because of the formation of a high degree of crystalline AS samples under shocked conditions, and similar kinds of results have been found under shocked conditions.[27]

FE-SEM Results. To provide considerably convincing evidence for the shock wave-induced dynamic recrystallization process occurring within milliseconds in the AS sample, FE-SEM analysis has been performed such that the obtained micrographs are portrayed in Figures 6 and 7. First, the 5 μm-scale micrographs of the control and shocked AS samples are provided in Figure 6, wherein the first row of Figure 6a–c shows the captured image, the 3D surface diagram, and the edge distribution image, respectively; a similar pattern has been followed for the 50- and 100-shocked samples, and the required images are presented in the second and third rows of Figure 6. The control sample exhibits small irregularly shaped particles, whereas at the 50-shocked condition, a significant modification in the surface and size of the particles could be seen and, most importantly, the shapes of the surface particles

are completely changed. For instance, any particle edge could not be seen, which may be because the surface might have undergone the premelting stage and crystallized with the surface particle's fusion, wherein the premelting might have occurred because of the lower thermal conductivity and diffusivity of the AS samples. Note that while the sample has low thermal energy transportation, during the shocked conditions, the applied thermal energy provides the required latent heat to melt the samples, but because of the occurrence of an immediate cooling process, recrystallization takes place. More simplifying, during the shocked conditions, shear-induced mechanical melting results in the formation of a nonequilibrium molten state which is highly unstable, and within fractions of milliseconds, the melt portion is recrystallized and is associated with both the temperature and local-order parameters. It is crucial that the shock wave-induced superheating and premelting stages fall under the non-equilibrium thermodynamic characteristics, and hence, the equilibrium thermodynamic characteristics such as melting point, critical phase transition temperature, and the test material's features could not be compared.[3,4,20−22]

Surprisingly, at the 100-shocked condition, highly defined characteristic surface morphological patterns of the AS samples could be seen (Figure 6g−i), wherein Figure 6i shows well-defined edges of the crystalline particle, which clearly represent the occurrence of dynamic recrystallization; the particles are retained with a highly ordered crystalline nature compared to the control sample, and as a result, a different possibility of a fast homogeneous nucleation under strongly superheated conditions by acoustical shock waves could be observed. Note that, as seen in Figure 6g−i, only the (200) prismatic facets' particles have the dominant morphological features compared to the other facets, and these results are found to be in good agreement with the XRD results. From the particle size distribution for the control and shocked samples seen in Figure 7, the 100-shocked sample was found to have a bigger particle size compared to the other samples due to the higher degree of crystallinity.

Based on the obtained results, it is quite clear that the (200) prismatic facets' particles are only along the preferable

orientation under shocked conditions. It has to be realized that the observed dynamic recrystallization is the combination of superheating and subsequent rapid cooling, which causes new stress-free crystals, wherein the observed crystal matrix (200) itself is stress-free. For premelting nucleation in a superheated crystal, an increase in superheating could increase both the driving force and the diffusivity, which will lead to a monotonic increment of the nucleation rate, and because of this reason, highly homogeneous crystals are observed at the 100-shocked condition, but it is suspected that this relationship is not linear as the temperature or number of shock pulses increases further. In addition to that, in Figure 8, the previously reported crystal morphologies are presented with the nomenclature of specific faces of the AS crystal (Figure 8a,b).[22] Figure 8c represents the conventional crystal growth-assisted AS sample, Figure 8d corresponds to the ultrasonic wave-assisted growth of the AS sample,[33] and Figure 8e represents the acoustical shock wave-assisted growth of the AS sample. As seen in Figure 8, the shock wave-induced recrystallized AS samples have the characteristics of the morphological patterns of the AS samples, which are found to be in good agreement with the conventional crystal growth-assisted AS sample.[22] Moreover, the shock wave-induced crystallization process is more dominant than that of the ultrasonic waves because of the distinct surface morphology and stress-free grain growth.

CONCLUSIONS

In this research, we successfully revealed the acoustical shock wave-induced dynamic recrystallization process of AS samples. The substantiation could be derived from the results obtained by the XRD, Raman, UV-DRS, and FE-SEM analyses, whereby it is established that the 100-shocked sample has a highly homogeneous and stress-free crystal surface along the (200) plane. Moreover, from the experimental outcome, we could demonstrate that for the superheated crystal, heterogeneous nucleation of premelting is avoided and that homogeneous nucleation might have played a dominant role in the melting kinetics. To date, for the first time, these results could substantiate the relationship between superheating and the attachment energy values of AS samples under acoustically shocked conditions in an unambiguous way. Henceforth, it is proposed that the present experimental results can serve as a reference for related research on the optimization of ammonium sulfate and other related typical chemical materials that undergo the dynamic recrystallization process.

ASSOCIATED CONTENT

Data Availability Statement

The data that support the findings of this study are available from the corresponding author upon reasonable request.

Supporting Information

The Supporting Information is available free of charge at https://pubs.acs.org/doi/10.1021/acs.cgd.3c01180.

> Additional experimental details of the shock wave-loading procedure (PDF)

AUTHOR INFORMATION

Corresponding Author

Lidong Dai − *Key Laboratory of High-Temperature and High-Pressure Study of the Earth's Interior, Institute of Geochemistry, Chinese Academy of Sciences, Guiyang,*

Guizhou 550081, China; orcid.org/0000-0002-9081-765X; Email: dailidong@vip.gyig.ac.cn

Authors

Sivakumar Aswathappa − *Key Laboratory of High-Temperature and High-Pressure Study of the Earth's Interior, Institute of Geochemistry, Chinese Academy of Sciences, Guiyang, Guizhou 550081, China*

S. Sahaya Jude Dhas − *Department of Physics, Kings Engineering College, Chennai 602 117 Tamilnadu, India*

S. A. Martin Britto Dhas − *Shock Wave Research Laboratory, Department of Physics, Abdul Kalam Research Center, Sacred Heart College, Tirupattur 635 601 Tamil Nadu, India;* orcid.org/0000-0003-0896-7534

Eniya Palaniyasan − *Department of Physics, Periyar University, Salem 636011 Tamil Nadu, India*

Raju Suresh Kumar − *Department of Chemistry, College of Science, King Saud University, Riyadh 11451, Saudi Arabia;* orcid.org/0000-0003-3754-4223

Abdulrahman I. Almansour − *Department of Chemistry, College of Science, King Saud University, Riyadh 11451, Saudi Arabia*

Complete contact information is available at:
https://pubs.acs.org/10.1021/acs.cgd.3c01180

Author Contributions

L.D. conceived the idea and led the project. S.A. performed the acoustic shock wave measurements. L.D., S.A., S.S.J.D., S.A.M.B.D. E.P., R.S.K., and A.I.A. contributed to the analysis, interpretation, and discussion of results. S.A. wrote the manuscript with the help of all of the authors. All of the authors commented on the final manuscript. L.D. supervised the project.

Notes

The authors declare no competing financial interest.

ACKNOWLEDGMENTS

REFERENCES

(1) Dandekar, P.; Kuvadia, Z. B.; Doherty, M. F. Engineering Crystal Morphology. *Annu. Rev. Mater. Res.* **2013**, *43*, 359.

(2) Springborg, M.; Zhou, M.; Molayem, M.; Kirtman, B. Surfaces, Shapes, and Bulk Properties of Crystals. *J. Phys. Chem. C* **2018**, *122*, 11926.

(3) Luo, S. N.; Ahrens, T. J. Shock-induced superheating and melting curves of geophysically important minerals. *Phys. Earth Planet. Inter.* **2004**, *143−144*, 369.

(4) Sakai, T.; Belyakov, A.; Kaibyshev, R.; Miura, H.; Jonas, J. J. Dynamic and post-dynamic recrystallization under hot, cold and severe plastic deformation conditions. *Prog. Mater. Sci.* **2014**, *60*, 130.

(5) Shen, Y.; Jester, S. B.; Qi, T.; Reed, E. J. Nanosecond homogeneous nucleation and crystal growth in shock-compressed SiO$_2$. *Nat. Mater.* **2016**, *15*, 60.

(6) Barber, E. R.; Ward, M. R.; Ward, A. D.; Alexander, A. J. Laser-induced nucleation promotes crystal growth of anhydrous sodium bromide. *CrystEngComm* **2021**, *23*, 8451.

(7) Turneaure, S. J.; Sharma, S. M.; Gupta, Y. M. Nanosecond Melting and Recrystallization in Shock-Compressed Silicon. *Phys. Rev. Lett.* **2018**, *121*, No. 135701.

(8) Renganathan, P.; Gupta, Y. M. Shock compression/release of magnesium single crystals along a low-symmetry orientation: Role of basal slip. *J. Appl. Phys.* **2019**, *126*, No. 115902.

(9) Vasu, K.; Matte, H. S. S. R.; Shirodkar, S. N.; Jayaram, V.; Reddy, K. P. J.; Waghmare, U. V.; Rao, C. N. R. Effect of high-temperature shock-wave compression on few-layer MoS_2, WS_2 and $MoSe_2$. *Chem. Phys. Lett.* **2013**, *582*, 105.

(10) Devika, M.; Reddy, N. K.; Jayaram, V.; Reddy, K. P. J. Sustainability of aligned ZnO nanorods under dynamic shock-waves. *Adv. Mater. Lett.* **2017**, *8*, 398.

(11) Kalaiarasi, S.; Sivakumar, A.; Dhas, S. A. M.; Jose, M. Shock wave induced anatase to rutile TiO2 phase transition using pressure driven shock tube. *Mater. Lett.* **2018**, *219*, 72.

(12) Sivakumar, A.; Sahaya Jude Dhas, S.; Chakraborty, S.; Kumar, R. S.; Almansour, A. I.; Arumugam, N.; Dhas, S. A. M. Dynamic Shock Wave-Induced Amorphous-to-Crystalline Switchable Phase Transition of Lithium Sulfate. *J. Phys. Chem. C* **2022**, *126*, 3194−3201.

(13) Mowlika, V.; Naveen, C. S.; Phani, A. R.; Sivakumar, A.; Dhas, S. A. M.; Robert, R. Shock wave induced magnetic phase transition in cobalt ferrite nanoparticles. *Mater. Chem. Phys.* **2022**, *275*, No. 125300.

(14) Sivakumar, A.; Sarumathi, M.; Sahaya Jude Dhas, S.; Dhas, S. A. M. Enhancement of the optical properties of copper sulfate crystal by the influence of shock waves. *J. Mater. Res.* **2020**, *35*, 391.

(15) Sivakumar, A.; Suresh, S.; Balachandar, S.; Thirupathy, J.; Kalyana Sundar, J.; Dhas, S. A. M. Effect of shock waves on thermophysical properties of ADP and KDP crystals. *Opt. Laser Technol.* **2019**, *111*, 284.

(16) Sivakumar, A.; Sahaya Jude Dhas, S.; Balachandar, S.; Dhas, S. A. M. Effect of shock waves on structural and dielectric properties of ammonium dihydrogen phosphate crystal. *Z. Kristallogr. - Cryst. Mater.* **2019**, *234*, 557−567.

(17) Bosetti, L.; Ahn, B.; Mazzotti, M. Study of Secondary Nucleation by Attrition of Potassium Alum Crystals Suspended in Different Solvents. *Cryst. Growth Des.* **2022**, *22*, 87−97.

(18) Mirsaleh-Kohan, N.; Fischer, A.; Graves, B.; Bolorizadeh, M.; Kendepudi, D.; Compton, R. N. Laser Shock Wave Induced Crystallization. *Cryst. Growth Des.* **2017**, *17*, 576.

(19) Thanh, N. T. K.; Maclean, N.; Mahiddine, S. Mechanisms of nucleation and growth of nanoparticles in solution. *Chem. Rev.* **2014**, *114*, 7610.

(20) Li, L.; Huang, B.; Zhang, G.; Wang, D.; Dai, M.; Yang, Z.; Wang, C. Optimization of ammonium sulfate crystals based on orthogonal design. *J. Cryst. Growth* **2021**, *570*, No. 126217.

(21) Malec, L. M.; Brela, M. Z.; Stadnicka, K. M. Displacive or Order-Disorder Phase Transition? The H-bond Dynamics in Multicaloric Ammonium Sulfate. *Acta Mater.* **2021**, *209*, No. 116782.

(22) Buchfink, R.; Schmidt, C.; Ulrich, J. Fe^{3+} as an example of the effect of trivalent additives on the crystallization of inorganic compounds, here ammonium sulfate. *CrystEngComm* **2011**, *13*, 1118.

(23) Sivakumar, A.; Balachandar, S.; Dhas, S. A. M. Measurement of "Shock Wave Parameters" in a Novel Table-Top Shock Tube Using Microphones. *Hum. Factors Mech. Eng. Def. Saf.* **2020**, *4*, 3.

(24) Shim, H. M.; Kim, J. W.; Koo, K. K. Molecular interaction of solvent with crystal surfaces in the crystallization of ammonium sulfate. *J. Cryst. Growth* **2013**, *373*, 64.

(25) Klitou, P.; Rosbottom, I.; Karde, V.; Heng, J. Y. Y.; Simone, E. Relating Crystal Structure to Surface Properties: A Study on Quercetin Solid Forms. *Cryst. Growth. Des.* **2022**, *22*, 6103.

(26) Liu, Y.; Niu, S.; Lai, W.; Yu, T.; Ma, Y.; Gao, H.; Zhao, F.; Ge, Z. Crystal morphology prediction of energetic materials grown from solution: insights into the accurate calculation of attachment energies. *CrystEngComm* **2019**, *21*, 4910.

(27) Sivakumar, A.; Saranraj, A.; Sahaya Jude Dhas, S.; Showrilu, K.; Dhas, S. A. M. Phase stability analysis of shocked ammonium dihydrogen phosphate by X-ray and Raman scattering studies. *Z. Kristallogr. - Cryst. Mater.* **2021**, *236*, 1−10.

(28) Sivakumar, A.; Sahaya Jude Dhas, S.; Sivaprakash, P.; Vigneshwaran, B.; Arumugam, S.; Dhas, S. A. M. Diffraction and spectroscopic assessment of crystallographic phase stability of potassium dihydrogen phosphate at shocked conditions. *Phys. B* **2022**, *627*, No. 413549.

(29) Salter, E. A.; Wierzbicki, A.; Land, T. Ab initio studies of stepped {100} surfaces of KDP crystals. *Int. J. Quantum Chem.* **2004**, *100*, 740.

(30) Schutte, C. J. H.; Heyns, A. M. Low-Temperature Studies. IV. The Phase Transitions of Ammonium Sulfate and Ammonium-d_4 Sulfate; the Nature of Hydrogen Bonding and the Reorientation of the NX^{4+} Ions. *J. Chem. Phys.* **1970**, *52*, 864.

(31) Unruh, H. G.; Ayere, O. Raman and dielectric measurements on ferrielectric ammonium sulphate. *Ferroelectrics* **1976**, *12*, 181.

(32) Abu El-Fadl, A.; Bin Anooz, S. Optical properties of pure and metal ions doped ammonium sulfate single crystals. *Cryst. Res. Technol.* **2006**, *41*, 487.

(33) Mohod, A. V.; Gogate, P. R. Improved crystallization of ammonium sulphate using ultrasound assisted approach with comparison with the conventional approach. *Ultrason. Sonochem.* **2018**, *41*, 310.